

Simulation domain

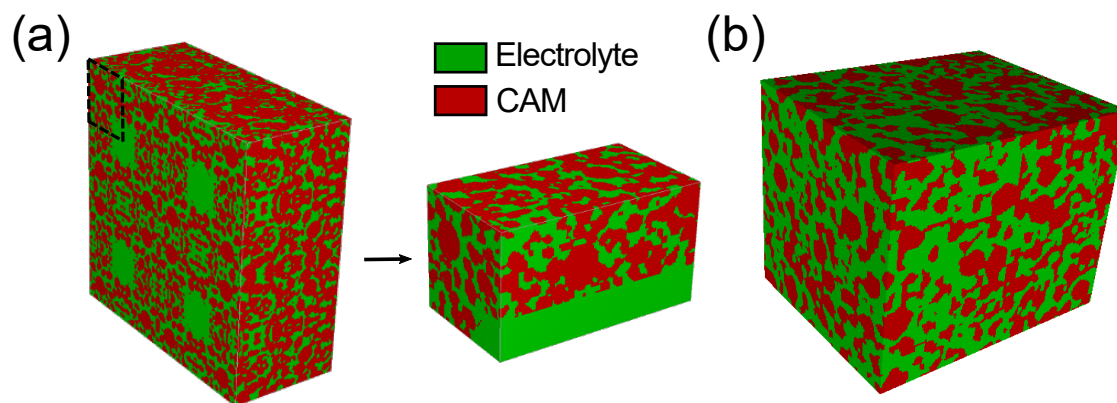


Figure S1: Overview of the generated 3D cathode structures. (a) Perforated cathode concept: To reduce computational costs, a quarter hole is simulated by taking advantage of the symmetry of the perforation pattern. (b) Layered cathode concept: A two-layered concept is investigated, with a first layer containing 60 vol% CAM at the separator side and a second layer containing 70 vol% CAM at the current-collector side.

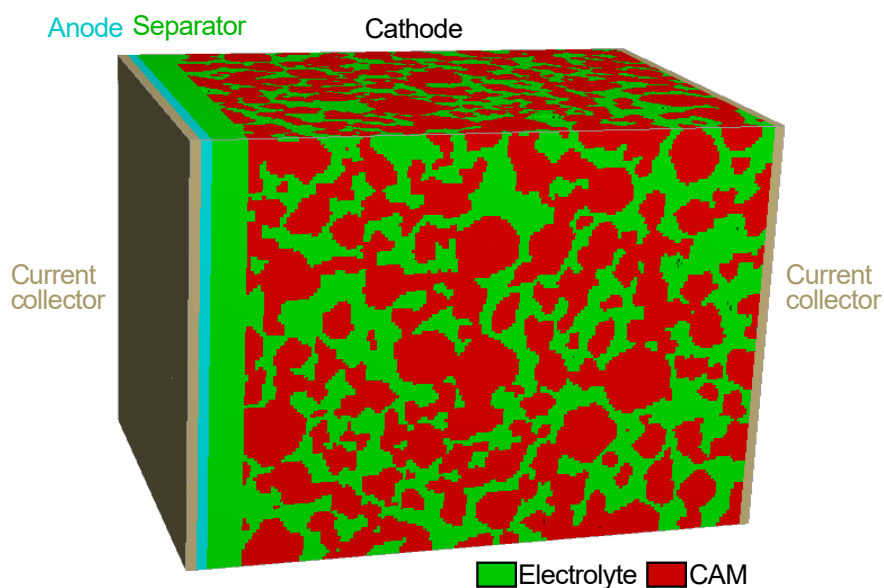


Figure S2: Overview of the input geometry for the structure-resolved simulations. A planar anode, separator, and current collectors are added to the generated cathode structures.

Parametrization

Table S1: Parameters of the electrochemical simulations. Functional parameters are indicated by * and are given at initial conditions.

Symbol	Value	Unit	Short description	Reference
Li-metal				
U_0^{An}	0	V	Open circuit potential	-
$\sigma_{\text{Li}}^{\text{An}}$	1	S/cm	Electronic conductivity	-
i_0^{Li}	$2.59 \cdot 10^{-2}$	A/cm^2	Exchange current density	[1]
α^{Li}	0.5	-	Symmetry factor	[2]
NMC 811				
U_0^{CAM}	4.2	V	Open circuit potential*	[3]
$c_{\text{Li}}^{\text{CAM},0}$	0.01131	mol/cm^3	Initial concentration of Li-ions	Calc.
$c_{\text{Li}}^{\text{CAM},max}$	0.04903	mol/cm^3	Maximum concentration of Li-ions	Calc.
$\sigma_{\text{Li}}^{\text{CAM}}$	$8.83 \cdot 10^{-3}$	S/cm	Electronic conductivity*	[4]
$D_{\text{Li}}^{\text{CAM}}$	LE: $1.63 \cdot 10^{-12}$ SE: $8.71 \cdot 10^{-13}$	cm^2/s	Li-ion diffusion coefficient*	[5]
i_{00}^{CAM}	LE: $2.402 \cdot 10^{-2}$ SE: $1.5392 \cdot 10^{-3}$	$\frac{Acm^{2.5}}{mol^{1.5}}$	Exchange current density factor	Calc. from [5]
LE (LiPF₆)				
$c_{\text{Li}}^{\text{LE}}$	$1 \cdot 10^{-3}$	mol/cm^3	Concentration of Li-ions	-
$\kappa_{\text{Li}}^{\text{LE}}$	$9.4 \cdot 10^{-3}$	S/cm	Li-ion bulk conductivity*	[6]
$D_{\text{Li}}^{\text{LE}}$	$3.79 \cdot 10^{-6}$	cm^2/s	Li-ion diffusion coefficient*	[6]
t_{Li}^+	0.25	-	Transference number*	[6]
TDF	1.85	-	Thermodynamic factor*	[7]
l_{sep}	20	μm	Separator thickness	-
SE (Li₆PS₅Cl)				
$c_{\text{Li}}^{\text{SE}}$	0.036662	mol/cm^3	Concentration of Li-ions	Calc.
$\kappa_{\text{Li}}^{\text{SE}}$	$0.7 \cdot 10^{-3}$	S/cm	Li-ion bulk conductivity	[5]
t_{Li}^+	1	-	Transference number	-
l_{sep}	20	μm	Separator thickness	-
Operation				
U_{cut}	3.0	V	Cut-off voltage	-

Performance indicators

From our simulation results, we derive several performance indicators that are crucial for identifying limiting processes and evaluating cathode designs.

Effective ionic conductivity The effective ionic conductivity of the cathode structures κ_{eff} is determined by solving the Poisson equation for the electrolyte phase. We apply a voltage of $U = 1$ V at the boundaries of the structure. From the resulting current density i and the length of the cathode l , the effective ionic conductivity can be calculated using Eq. S1.

$$\kappa_{\text{eff}} = l \cdot \frac{i}{U} \quad (\text{S1})$$

Theoretical capacity The theoretical capacity of the cathode structures is calculated based on their CAM fraction (Eq. S2). c_0 and c_{max} are the initial and maximum concentration of Li-ions in the CAM. F is the Faraday constant. A is the current collector area and V_{CAM} the CAM volume in the composite cathode.

$$C_{\text{theo}} = \frac{(c_{\text{max}} - c_0) \cdot F \cdot V_{\text{CAM}}}{A} \quad (\text{S2})$$

Energy density An important performance indicator is the energy density E_{grav} of the battery cell, given by Eq. S3. The mass of the separator m_{Sep} and cathode m_{Ca} are deduced from the input microstructure used in our simulations. The anode mass m_{An} is estimated, assuming an ideal matching between the negative and positive electrode. Please note that we neglect the weight of current collectors and cell housing. i and U are the current density and cell voltage, respectively. The additional parameters used to calculate the energy density

are summarized in Table S2.

$$E_{\text{grav}} = \frac{\int_{t_0}^{t_{\text{end}}} i \cdot U dt}{m_{\text{An}} + m_{\text{Sep}} + m_{\text{Ca}}} \quad (\text{S3})$$

CAM utilization The utilization of the CAM η_{CAM} can be evaluated from the current Li-ion concentration in the CAM c_{CAM} through Eq. S4. $c_{\text{CAM},0}$ and $c_{\text{CAM,max}}$ are the initial and maximum concentration of Li-ions, respectively.

$$\eta_{\text{CAM}} = \frac{c_{\text{CAM}} - c_{\text{CAM},0}}{c_{\text{CAM,max}} - c_{\text{CAM},0}} \quad (\text{S4})$$

Table S2: Parameters used for the calculation of gravimetric capacity and energy density.

Symbol	Value	Unit	Short description	Reference
Li-metal				
$C_{\text{grav,Li}}^{\text{theo}}$	3861	mAh/g	Theoretical gravimetric capacity	[8]
SE (Li₆PS₅Cl)				
ρ_{SE}	1.64	g/cm^3	Gravimetric density	[9]
NMC 811				
ρ_{CAM}	4.77	g/cm^3	Gravimetric density	[3]

Perforated cathodes

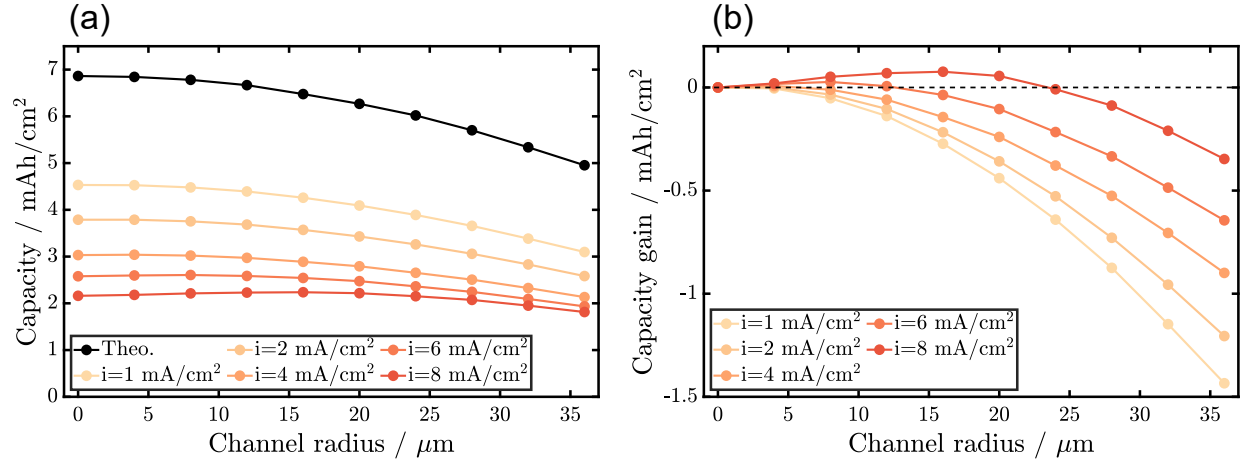


Figure S3: Effect of channel radius on capacity for the ASSB case. (a) Capacity for various current densities. The black line represents the theoretical capacity of the perforated structures. (b) Capacity gain of perforated structures at different current densities compared to the non-perforated structure ($r_{\text{channel}} = 0 \mu\text{m}$).

Layered cathodes

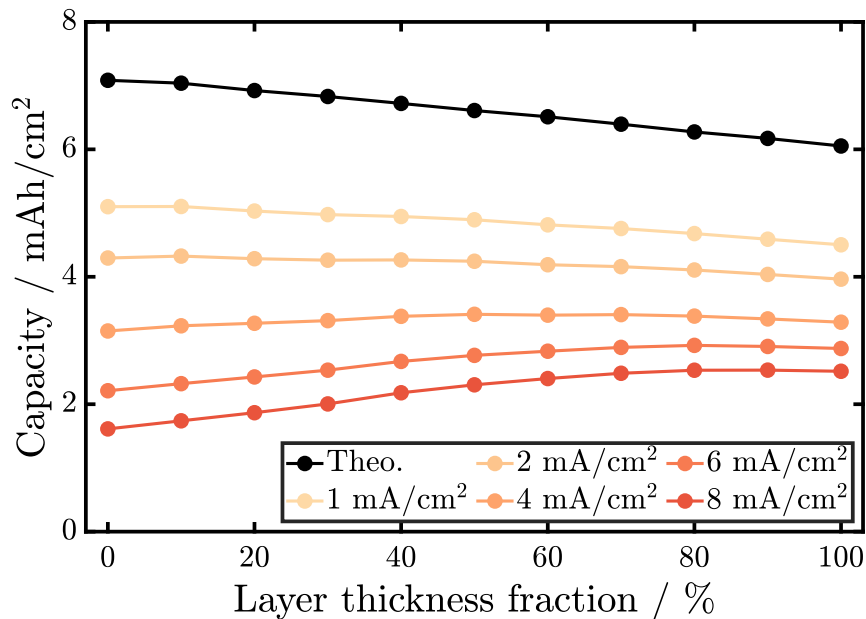


Figure S4: Influence of layer thickness fraction on ASSB capacity. Current densities range from 1 to 8 mA/cm². The black line represents the theoretical capacity of the generated structures.

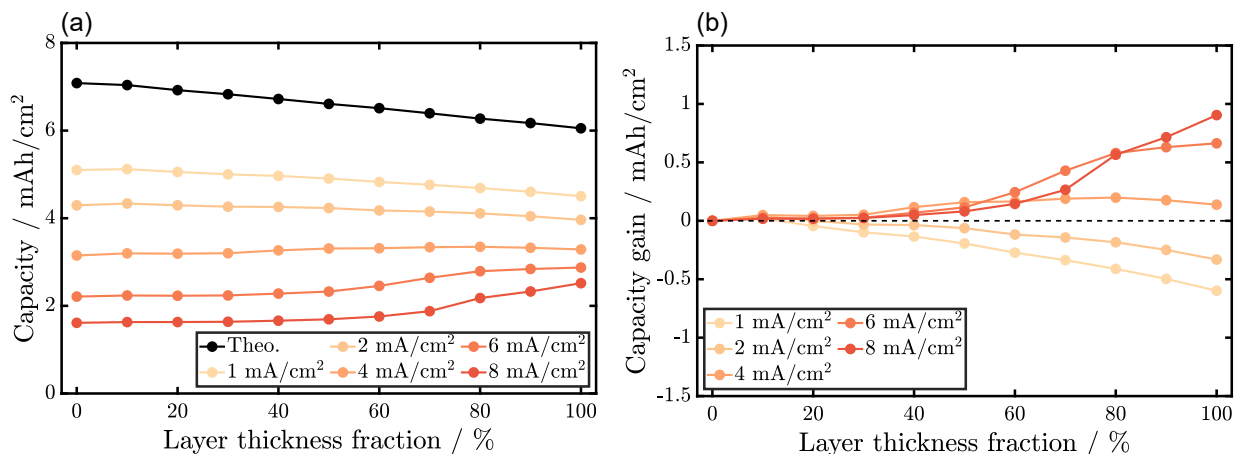


Figure S5: Influence of layer thickness fraction of the two-layered cathodes on electrochemical ASSB performance. The generated structures were reversed to show the significance of reducing tortuosity in the SE phase close to the separator. In the reversed structures, CAM loading is increased at the separator side and reduced at the current collector side of the cathode. (a) Capacity for current densities ranging from 1 to 8 mA/cm². The black line represents the theoretical capacity of the generated structures. (b) Capacity gain realized for the layered structures compared to a homogeneous cathode structure with 70 vol% CAM ($f_{L60} = 0$).

References

- (1) Neumann, A.; Hamann, T. R.; Danner, T.; Hein, S.; Becker-Steinberger, K.; Wachsmann, E.; Latz, A. Effect of the 3D structure and grain boundaries on lithium transport in garnet solid electrolytes. *ACS Appl. Energy Mater.* **2021**, *4*, 4786–4804.
- (2) Finsterbusch, M.; Danner, T.; Tsai, C.-L.; Uhlenbruck, S.; Latz, A.; Guillon, O. High capacity garnet-based all-solid-state lithium batteries: fabrication and 3D-microstructure resolved modeling. *ACS Appl. Mater. Interfaces* **2018**, *10*, 22329–22339.
- (3) Bielefeld, A.; Weber, D. A.; Rueß, R.; Glavas, V.; Janek, J. Influence of lithium ion kinetics, particle morphology and voids on the electrochemical performance of composite cathodes for all-solid-state batteries. *J. Electrochem. Soc.* **2022**, *169*, 020539.
- (4) Amin, R.; Chiang, Y.-M. Characterization of electronic and ionic transport in $\text{Li}_{1-x}\text{Ni}_{0.33}\text{Mn}_{0.33}\text{Co}_{0.33}\text{O}_2$ (NMC333) and $\text{Li}_{1-x}\text{Ni}_{0.50}\text{Mn}_{0.20}\text{Co}_{0.30}\text{O}_2$ (NMC523) as a function of Li content. *J. Electrochem. Soc.* **2016**, *163*, A1512.
- (5) Ruess, R.; Schweidler, S.; Hemmelmann, H.; Conforto, G.; Bielefeld, A.; Weber, D. A.; Sann, J.; Elm, M. T.; Janek, J. Influence of NCM particle cracking on kinetics of lithium-ion batteries with liquid or solid electrolyte. *J. Electrochem. Soc.* **2020**, *167*, 100532.
- (6) Nyman, A.; Behm, M.; Lindbergh, G. Electrochemical characterisation and modelling of the mass transport phenomena in LiPF_6 -EC-EMC electrolyte. *Electrochim. Acta* **2008**, *53*, 6356–6365.
- (7) Landesfeind, J.; Gasteiger, H. A. Temperature and concentration dependence of the ionic transport properties of lithium-ion battery electrolytes. *J. Electrochem. Soc.* **2019**, *166*, A3079–A3097.
- (8) Xu, W.; Wang, J.; Ding, F.; Chen, X.; Nasybulin, E.; Zhang, Y.; Zhang, J.-G. Lithium metal anodes for rechargeable batteries. *Energy Environ. Sci.* **2014**, *7*, 513–537.

(9) Materials data on $\text{Li}_6\text{PS}_5\text{Cl}$ by Materials Project, DOI: 10.17188/1316731. 2020.